PROPERTIES OF REISSNER FIBER ASSEMBLY AND SIGNALING DURING BODY AXIS STRAIGHTENING

by

SOPHIE FISHER

A THESIS

Presented to the Department of Neuroscience
and the Robert D. Clark Honors College
in partial fulfillment of the requirements for the degree of
Bachelor of Science

April 2024

An Abstract of the Thesis of

Sophie Fisher for the degree of Bachelor of Science
in the Department of Neuroscience to be taken June 2024

Title: Properties of Reissner Fiber Assembly and Signaling During Body Axis Straightening

Approved: *Prof. Daniel T. Grimes*
Primary Thesis Advisor

Spinal conditions like scoliosis are highly prevalent across the globe. However, not much is known about how the spine develops its symmetrical shape and maintains that shape throughout adulthood. In this thesis, I used zebrafish as a model organism to study early body straightening and how zebrafish maintain their straight spine throughout adulthood.

Chapter I focuses on understanding the Reissner fiber, a proteinaceous fiber that sits in the zebrafish central canal of the spinal cord. The central canal is lined with motile cilia, which generate a fluid flow that promotes the formation of the Reissner fiber. Like motile cilia, the Reissner fiber is an important component for both early body straightening and maintaining a straight spine throughout life. It is primarily composed of the glycoprotein SCOspondin. However, other potential components of the Reissner fiber may act in axial straightening. One of these candidates are F-spondin proteins, Spon1a and Spon1b. To test if these proteins are important in early axial straightening, I generated somatic mutants using CRISPR/Cas9 to knock out the genes that encode Spon1a and Spon1b. I found that neither Spon1a nor Spon1b were required for axial straightening, so they are not likely relevant to developing a straight body axis. Mutation of these genes also did not disrupt the integrity of the Reissner fiber, adding further evidence that F-spondin proteins are not critical for spinal development.

After examining F-spondin proteins, I wanted to further investigate the Reissner fiber. Therefore, my second experiment in Chapter I examined the dynamics of Reissner fiber assembly, a largely unknown topic. To investigate this, I generated SCOspondin mosaic mutants using CRISPR/Cas9. In these mutants, the central canal of the zebrafish had some cells that could produce SCOspondin while some that couldn't, allowing me to examine whether assembly relied on local secretion of SCOspondin, or if the protein aggregated to form the Reissner fiber in a more distributed fashion. I found that Reissner fiber assembly relied on two factors. First, there had to be enough SCOspondin in the central canal above a threshold. I also found that the Reissner fiber could form over gaps of floor plate cells that couldn't produce SCOspondin, supporting a distributed model of assembly

Chapter II focuses on signaling downstream of the Reissner fiber, namely the role of Urotensin-II peptides (Urps). Urps have recently emerged as a factor that mediates spine morphology that acts downstream of the Reissner fiber; however, less is known about their role in maintaining a straight spine throughout adolescence and adulthood. Therefore, we generated germline mutants that lacked Urp 1, Urp 2, both Urp 1 and Urp 2, or the Urp receptor. We found that while Urps were not necessary for proper body straightening early in development, zebrafish lacking these peptides developed spinal curves during adolescent growth stages. The spinal curves in urotensin mutants worsened into adulthood, but showed a distinct phenotype compared to motile cilia mutants. Because the phenotypes of urotensin and motile cilia mutants do not match, this indicates that Urps are not the only factor acting downstream of motile cilia to control spine morphology.

Overall, this thesis adds to the current model of early axial straightening and adult spine morphology. Chapter I ruled out potential proteins from the model and explored the dynamics of

Reissner fiber assembly. Chapter II explored the important role of Urps in maintaining a straight spine throughout life. Ultimately, this information can help us understand human spinal conditions like scoliosis.

Acknowledgements

I would like to thank all members of the Grimes Lab for supporting my time in lab over the past three years. Particularly, I would like to thank Professor Grimes, for offering me a place and opportunity to learn about research and Beth Bearce for teaching me so much about scientific research and devoting so much time to help me. I would also like to thank Beth for allowing me to include several of their contributions to present a more complete story, particularly in chapter II. I am excited to take everything I have learned about scientific research into the next phase of my life. I would also like to thank Judy Peirce for assisting me with several fish experiments. Last, I would like to thank Nicole Dudukovic for her support and taking the time to be on my thesis committee.

Table of Contents

List of Figures

Chapter I: Characterizing the Reissner Fiber

Introduction

Zebrafish as a Model Organism for Idiopathic Scoliosis

Adolescent idiopathic scoliosis (AIS) is a common spinal pathology affecting upwards of 3% of the world population and is characterized by abnormal, lateral curvature of the spine that arises during adolescence [1]. Despite its prevalence, its etiology remains largely unknown. Zebrafish (*Danio rerio*) have recently emerged as a suitable model organism to study both AIS and early spinal development due to their natural susceptibility to spinal curvatures[1]. Unlike quadrupeds, which are commonly used in scientific research, the mechanical load on the zebrafish spine during swimming is thought to be more similar to that of humans[2]. Further, zebrafish have a short developmental window which allows for more efficient experimentation and are transparent in early development allowing for easy observation of internal processes. By uncovering the mechanisms underlying the development and maintenance of a straight spine in zebrafish, information on the mechanisms behind human scoliosis may be uncovered.

Body Straightening in Zebrafish

Zebrafish develop their characteristic straight body axis during the segmentation period. During this period from 10-24 hours post fertilization (hpf), the primary organs become visible, and the tail bud appears at the caudal end of the zebrafish[3]. Throughout the beginning of this period, the zebrafish grows around its yolk, a membranous developmental sac, and towards its head[3]. During axis elongation, the tail detaches from the yolk and straightens to generate the linear body axis[3]. The various mechanisms that govern this early body elongation also appear to

be relevant to adult spine morphology, making early body axis straightening a tractable surrogate model for later spine maintenance.

Critical components for developing a straight body axis in early development and maintaining it through later growth phases are motile cilia. Motile cilia are microtubule-based structures that project off cellular membranes[4]. They contain axonemal dynein arms which are large multi-protein complexes[5]. These arms hydrolyze ATP to power the beating of the cilium[5]. Motile cilia are important for a variety of functions like powering the propulsion of sperm cells and moving particles across epithelial cells through the generation of fluid flows[6]. For example, motile cilia in the airways generate a flow of mucus, clearing the airways of debris.

Motile cilia must be correctly formed and oriented properly to generate directional fluid flows. In zebrafish, motile cilia line the brain ventricles and central canal, a lumen inside of the spinal cord[4]. Within the central canal, motile cilia generate a bidirectional fluid flow of cerebrospinal fluid (CSF), a clear fluid that bathes the brain and spinal cord[4]. When motile cilia are mutated to compromise their motility, CSF flow is reduced, and ventral axis curves develop in zebrafish embryos[7], a phenotype referred to as curly tail down. However, motile cilia are not only important for early axial straightening, but also the maintenance of a straight spine throughout adolescence. For example, by employing the temperature-sensitive motile cilia mutant, *cfap298*, zebrafish can be raised in permissive conditions, but when moved to higher temperatures during juvenile growth phases, they develop spinal curves[8]. Therefore, motile cilia and the CSF flow they generate appear to be important for early axial straightening and the maintenance of a straight spine after development.

The Reissner Fiber

The Reissner fiber is a key component of the central canal that is thought to play a role downstream of motile cilia in axial straightening. The Reissner fiber is a thread-like structure that spans the central canal of the spinal cord and is primarily composed of the glycoprotein SCOspondin, encoded by *sspo.* It is initially produced and secreted by cells of the floor plate and, later, the sub-commissural organ (SCO)[9]. When zebrafish were generated without SCOspondin, through CRISPR mutagenesis, the Reissner fiber did not form and mutants were found to have curly tail down, the same as motile cilia mutants[10]. However, cilia motility and CSF flow were not disrupted in *sspo* mutants, suggesting that motile cilia and CSF flow are an upstream step in axial straightening[10]. This indicates that motile cilia-generated fluid flow is responsible for the formation of the Reissner fiber, potentially by mediating SCOspondin aggregation and organization into a fiber.

The Reissner fiber may interact with CSF-contacting neurons (CSF-cNs) which project into the lumen of the central canal. CSF-cNs are GABAergic sensory neurons with an apical cilium, as well as stereocilia bundles, that extend into the central canal[4]. They are in close proximity, even in physical contact, with the Reissner fiber[11]. CSF-cNs are both mechanosensory and chemosensory. The CSF-cNs mechanosensory response relies on the Reisner fiber because *sspo* mutants that lack the fiber showed decreased calcium responses of CSF-cNs[11]. Therefore, the Reissner fiber and CSF-cNs may form a mechanosensory system that can detect spinal curvatures in the zebrafish. For example, if the zebrafish is bent too much in one direction, CSF-cNs would form a physical contact with the Reissner fiber and/or experience an enhancement of CSF flow, that would trigger their firing[11]. However, another idea is that CSF-cNs may mediate axial straightening through their chemosensory properties. For example, the Reissner fiber

interacts and binds with monoamines like epinephrine[12]. In this model, epinephrine transported down the Reissner fiber, from the brain to the central canal, might signal to CSF-cNs, causing firing when the Reissner fiber and CSF-cNs are in close proximity[2]. Factors acting downstream of this interaction to control axial straightening will be assessed in Part II.

Spon1a and Spon1b

F-spondin proteins are extracellular matrix proteins that were first characterized in rat floor plate cells and serve as another potential player in the axial straightening process[13]. They are expressed and secreted by the floor plate along with other parts of the nervous system and are thought to promote proper development of the central nervous system through neural cell adhesion and neurite outgrowth[13]. In zebrafish, Spon1a and Spon1b are the two F-spondin homologs[14]. Despite a 74% shared identity between the two zebrafish homologs[14], they are expressed during different developmental timepoints. *spon1b* mRNA expression begins at 9-10 hpf while *spon1a* mRNA expression onsets at 48 hpf[14]. Further, larval and adult zebrafish have a higher abundance of *spon1b* mRNA[14]. Spon1b is expressed diffusely throughout the zebrafish nervous system[14]. Particularly, the protein is expressed along the entire floor plate, which is the primary source for SCOspondin secretion during Reissner fiber assembly in the central canal prior to formation of the sub-commissural organ[10], and has particularly pronounced expression at the flexural organ which is a later source of Reissner fiber-related proteins[14]. It was also found to localize to a thread-like structure in the central canal resembling the Reissner fiber[15]. Therefore, F-spondin proteins may comprise part of the proteinaceous Reissner fiber. Further, given their role in CNS development, they may serve as a candidate for mediating axial straightening and interactions between the Reissner fiber and CSF-cNs[14]. It has not been tested whether F-spondins

function in Reissner fiber assembly or structure, or whether they participate in body axis morphology.

My Work

For my work in characterizing the Reissner fiber, I had two goals. First, to understand the importance of various potential components of the fiber. Therefore, I investigated the role of Spon1a and Spon1b in the structure of the Reissner fiber and the downstream axial straightening process. To accomplish this, I first generated zebrafish crispants that had deletions in the protein coding regions for either Spon1a, Spon1b, or both Spon1a and Spon1b in AB strain zebrafish to assess the effects of F-spondin disruption on body axis morphology. Additionally, I assessed the assembly and structural morphology of the Reissner fiber after F-spondin disruption by injecting the same crispant cocktails into fish with a GFP-tagged Reissner fiber that could be observed with live fluorescent microscopy. These experiments rely on *scospondin-GFP*^{ut24}, a zebrafish stock with an endogenous knock-in of green fluorescent protein (GFP) to the C-terminus of the *sspo*, which was generated by Ryan Gray's Lab at UT-Austin[16]. The body morphology and Reissner fiber assembly of these three crispants were compared to multiplex G0 crispants against *sspo* (as a positive control) or uninjected controls. Since little is known about how these proteins may support the Reissner fiber and modulate axial straightening, this is an important avenue of work to further our model of body shape development. Given that the onset of *spon1a* mRNA expression begins at 48hpf[14], I hypothesized that zebrafish lacking this protein would have an intact Reissner fiber and normal body axis phenotype. However, for zebrafish lacking Spon1b or both Spon1a and Spon1b, I hypothesized that there would be disruptions to the structure of the Reissner fiber and thus axial straightening defects because Spon1b is expressed during pertinent time periods of axial straightening.

I also performed experiments that sought to test how the Reissner fiber assembles from secreted SCOspondin. The goal was to explore how local SCOspondin secretion from the floorplate functions in assembly of the Reissner fiber. Particularly, whether this process relies on a constant, uninterrupted supply of secreted SCOspondin from the underlying floor plate. Given not much is known about the dynamics of Reissner fiber assembly, this experiment could further our understanding of how the Reissner fiber forms. Particularly, if the SCOspondin that the floor plate cells secrete amass to form the Reissner fiber at a highly local level in relation to their source, or if secreted SCOspondin can attach to the fiber and function at a distance from their site of secretion. To accomplish this, I generated zebrafish crispants in the *scospondin-GFP^{ut24}* line to induce mosaic mutations in *sspo*, meaning that not every floor plate cell would be able to produce SCOspondin. Given the dynamics of CSF flow in the central canal, I hypothesized that the Reissner fiber would be conserved in zebrafish that had a mosaic pattern of mutations to *sspo* and that they would have a typical body phenotype.

Methods

Zebrafish

Zebrafish embryos were attained from natural mating of either the AB strain or the *scospondin-GFP^{ut24}* strain (gift of Ryan Gray, UT-Austin). Experiments were approved by the University of Oregon Institutional Animal Care and Use Committee and followed the guidelines of the International Association for Assessment and Accreditation of Laboratory Animal Care. To investigate the role of Spon1a and Spon1b, crispants were generated in both the AB and *scospondin-GFP^{ut24}* strain. To generate mosaic zebrafish mutants, the *scospondin-GFP^{ut24}* strain was used and *sspo* crispants were generated.

gRNA Synthesis and CRISPR/Cas9 Mutagenesis

A look-up table provided the 4 gRNA oligos for *spon1a*, *spon1b*, and *sspo* somatic mutagenesis[17].

spon1a oligo sequences:	5'/TAATACGACTCACTATAGGGCAGGGTTTGTTGCATACGTTTTAGAGCTAGAAATAGC/3'; 5'/TAATACGACTCACTATAGGGTCACCTTCTACGGCAACGTTTTAGAGCTAGAAATAGC/3'; 5'/TAATACGACTCACTATAGGGTGGCGCAATTACTCCCGGTTTTAGAGCTAGAAATAGC/3'; 5'/TAATACGACTCACTATAGGTGAAAAGACGAGAGCGAAGTTTTAGAGCTAGAAATAGC/3'
spon1b oligo sequences:	5'/TAATACGACTCACTATAGGACGCAGGCGCGGAGCGCTGTTTTAGAGCTAGAAATAGC/3'; 5'/TAATACGACTCACTATAGGATGGATCACCCGTCAAAAGTTTTAGAGCTAGAAATAGC/3'; 5'/TAATACGACTCACTATAGGCGATATCGTCTATCGTGTGTTTTAGAGCTAGAAATAGC/3'; 5'/TAATACGACTCACTATAGGCAGCGCTTCATGCGGGATGTTTTAGAGCTAGAAATAGC/3'
sspo oligo sequences:	5'/TAATACGACTCACTATAGGAGCCTAGACCTGCTCACGGTTTTAGAGCTAGAAATAGC/3'; 5'/TAATACGACTCACTATAGGAGCCTAGACCTGCTCACGGTTTTAGAGCTAGAAATAGC/3'; 5'/TAATACGACTCACTATAGGAAACGGCCGTCAGTGTCGGTTTTAGAGCTAGAAATAGC/3'; 5'/TAATACGACTCACTATAGGAAACGGCCGTCAGTGTCGGTTTTAGAGCTAGAAATAGC/3'

Guide RNAs were generated for each target by first assembling oligos. First, equimolar concentrations of top oligos (10 µM each) were mixed. In a PCR strip, 1 µL of the diluted top oligos was mixed with 0.5 µL Phusion DNA polymerase, 25 µl 2x Phusion buffer +dNTPs, 22.5

µl nuclease-free water, and 1 µl of the bottom strand ultramer (10 µM). The oligo was then annealed and extended using a thermocycler with the following protocol: 98°C (2 min), 50°C (10 min), 72°C (10 min), 4°C (hold).

The assembled oligos were then purified using a Zymo Research DNA Clean & Concentrator-5 kit. After, the purified, assembled oligo was used for in vitro RNA synthesis using a NEB T7 High Yield kit. After four hours of incubation at 37°C, 1 µL of DNase was added and allowed to incubate for 15 minutes. The gRNA was purified using an RNA Clean & Concentrator Kit from Zymo Research. Individual aliquots of 3 µL each gRNA were stored at -80°C until use. For the use in mutagenesis, 1000 pg of gRNAs and 1600 pg/nl Cas9 was injected into one-cell-stage embryos. However, to generate mosaic crispants, a variety of concentrations of gRNA were used: 1000 pg, 500 pg, 100 pg, 10 pg, and 0 pg as a negative control.

Measuring Larval Body Curvature

Using a Leica S9i stereomicroscope with an integrated 10-megapixel camera, lateral views of zebrafish larvae were taken at 24 hours post fertilization. Body angles, denoted as θ, were quantified in ImageJ. Body angles were compared between each injection condition using unpaired t-tests. For mosaic crispants, body angles were compared between each injection concentration.

Confocal Microscopy

First, embryos (28 hpf) were anesthetized using tricaine until their touch response was eliminated. Subsequently, they were embedded in 0.8% low-melt agarose containing tricaine within inverted imaging chambers (14 mm #1.5 coverslips, VWR cat no. 10810–054). Images were captured in 512×256 timeseries using a Nikon Ti2 inverted microscope equipped with Plan Apo ×40 and ×60 WI DIC (1.2 NA) objectives, a Yokogawa Spinning Disk, and a pco.edge

sCMOS camera. Parameters such as exposure, camera settings, and laser power were standardized across embryos. Lastly, images were processed in ImageJ.

Plotting

All plots were generated using GraphPad version 10.2.0. In body angle plots, individual embryos are depicted by dots and population means plus/minus standard deviation by black lines. Each condition had multiple rounds of experimentation, so each trial is depicted in a different shade in the same color scheme for each condition.

Results

Mutation to F-spondin proteins did not disrupt body straightening

To investigate the role of Spon1a and Spon1b in the Reissner fiber and body straightening, I used CRISPR/Cas9 to knock out the Spon1a and Spon1b genes, generating crispants. Crispants are where the Cas9 protein generates multiple mutations throughout the gene of interest, effectively knocking it down in a mosaic fashion. This is in contrast to germline mutations where the mutation in the gene of interest is always the same and carried in every cell. In this experiment, I generated single crispants for *spon1a* and *spon1b*, and double crispants, *spon1a;spon1b*, where both Spon1a and Spon1b genes were mutated. As a positive control for my injections and Cas9, I also generated crispants that targeted *sspo*, the primary protein of the Reissner Fiber, as mutants are known to exhibit ventral axis curves that can be easily scored. I performed CRISPR/Cas9 injections in wild type (AB) zebrafish and *scospondin-GFP*^{ut24} fish. Zebrafish from the *scospondin-GFP*^{ut24} line have a fluorescent Reissner fiber which allowed me to image the integrity of the fiber in these crispants.

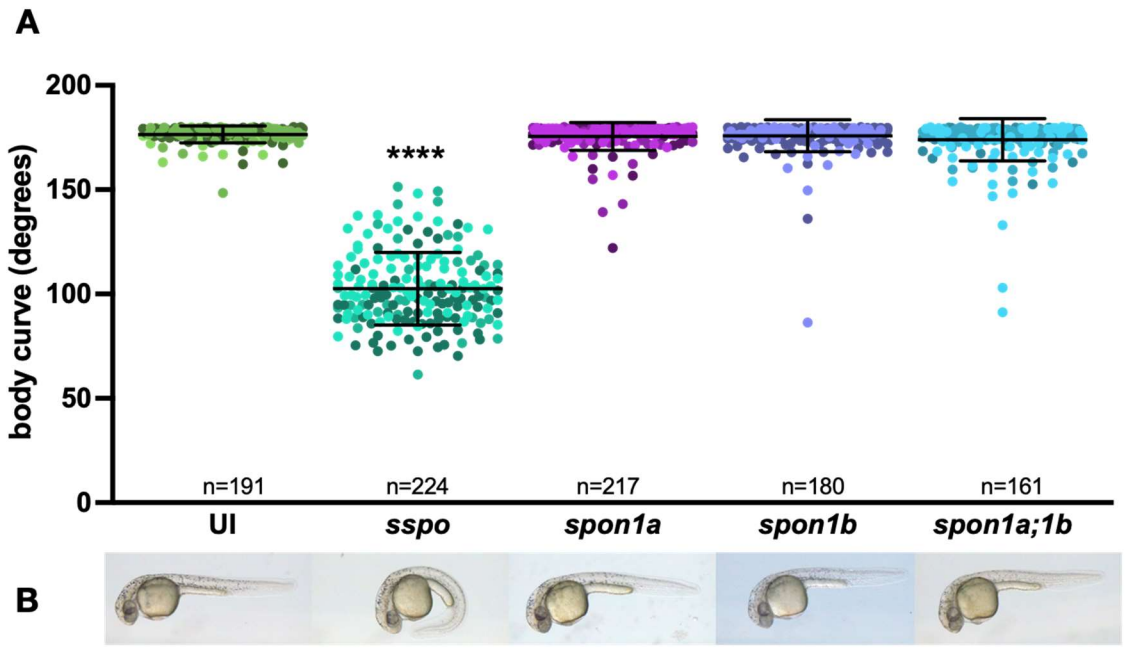

Figure 1: A) Superplot of body angle measurements for *sspo, spon1a, spon1b,* and *spon1a;1b* crispants of the AB strain. B) Lateral views of each condition at 28hpf.

A) Individual dots represent the body angle of an individual embryo at 28hpf, and black bars represent the mean ± SD. Total embryos injected is displayed on the figure and the experiment was repeated three times which is represented by distinct color shades for each condition. Each condition had a statistically significant difference from *sspo* ($p<0.0001$). UI = uninjected.

With an assay where I measured body curvature, crispants in which Spon1a, Spon1b, or both of these proteins were targeted, were not statistically different than uninjected zebrafish (figure 1). These crispants, along with uninjected zebrafish were significantly different than *sspo* crispants (figure 1), the positive control. Therefore, zebrafish crispants lacking F-spondin proteins were able to correctly develop a straight body axis.

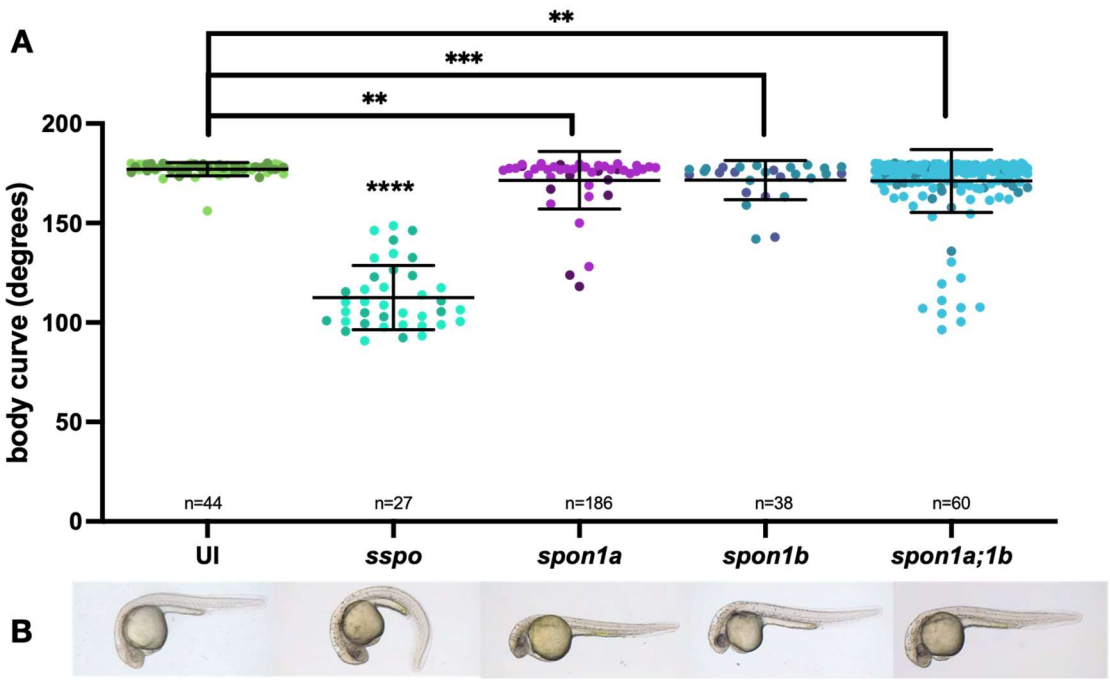

Figure 2: A) Superplot of body angle measurements for *sspo, spon1a, spon1b,* and *spon1a;1b* crispants of the *scospondin-GFP*^{ut24} strain. B) Lateral views of each condition at 28hpf.

A) Individual dots represent the body angle of an individual embryo at 28hpf, and black bars represent the mean ± SD. Total embryos injected is displayed on the figure and the experiment was repeated three times which is represented by distinct color shades for each condition. Each condition had a statistically significant difference from *sspo* ($p<0.0001$). Additionally, *spon1a, spon1b,* and *spon1a;spon1b* were also significantly different than UI ($p=0.0045$, 0.0002, and 0.0042 respectively). UI = uninjected.

Similarly to crispants of the AB strain, there was a significant difference between *sspo* crispants and all other crispants and uninjected zebrafish for the *scospondin-GFP*^{ut24} strain (figure 2). However, there were also significant differences, albeit at a lower level, for *spon1a, spon1b, spon1a;spon1b* crispants compared to uninjected (figure 2). This result is interesting because differences in phenotypes between the AB strain and *scospondin-GFP*^{ut24} strain were not expected. In fact, mutations were only induced in the *scospondin-GFP*^{ut24} strain in order to visualize the Reissner fiber, not as the primary experiment to measure body angles. These results may be influenced by a few outliers in these zebrafish clutches that exhibited curly tail down

phenotypes while the other fish had normal, straight phenotypes. When imaged using confocal microscopy, these crispants had in-tact Reissner fibers. However, the few outliers that did have a curly tail down phenotype did have disruptions to Reissner fiber integrity. It is possible that Spon1a and Spon1b do play small roles in Reissner fiber assembly and integrity, but this role is not large enough to induce a body axis curve in AB zebrafish. By contrast, I could be seeing occasional curves in *spon1a, spon1b*, and *spon1a;spon1b* crispants when generated in the *scospondin-GFP^{ut24}* background because the fiber is sub-optimal in this line owing to the main component, Sspo, carrying a GFP tag.

These results support either no role, or a minor role, for Spon1a and Spon1b in Reissner fiber formation and body curvature. To fully test this hypothesis, I would use molecular assays to determine the extent of mutagenesis I induced in crispants and, if time had allowed, I would generate germline mutants for analysis.

Local Disruption to Floor Plate Cells does not Disrupt the Reissner Fiber

When I generated *sspo* crispants in the *scospondin-GFP^{ut24}* line as a positive control for the previous experiment, an interesting result was noted, which became the focus of a second experiment. I observed that some of these fish had visible mosaicism in their expression of SCOspondin in the floor plate cells. This is to be expected, because crispant mutation strategies generate a host of variable mutations (near the targeted PAM site of the gene of interest) in different somatic cell populations—thus, crispant strategies are inherently mosaic. This is of utility for us, because we can use "patchy" expression of Sspo-GFP to test the local conditions that are required for Reissner fiber assembly. Therefore, I was intrigued by the possibility of intentionally generating the same *sspo* crispants with variable rates of mosaicism, in order to understand the dynamics of local assembly of the Reissner fiber in the central canal. I

hypothesized that the assembly of the Reissner fiber is local, occurring downstream of the activity of local motile cilia (i.e. that the fiber would not assemble if there were significant gaps in floor plate cells expressing Sspo-GFP). Thus, in areas of the central canal where Sspo-GFP expression is absent and local concentration of Sspo-GFP material is low, dynamics of Reissner fiber assembly would be impacted. However, given that central canal motile cilia generate fluid flow, it is also possible that bulk expression of Sspo-GFP in an anterior region of the canal would be able to compensate for a local reduction in Sspo-GFP secretion; thus, at some threshold, Reissner fiber assembly would persist in areas of the central canal that do not secrete the components for assembly. These two models can be considered as Sspo acting locally, near its site of secretion, or at a distance. To distinguish these models, I used CRISPR/Cas9 at progressively diluted concentrations to produce varying levels of SCOspondin reduction and mosaicism in the *scospondin-GFP*^{ut24} line where loss of GFP expression was interpreted as a cell with two non-functional copies of *sspo*. The goal was to generate a zebrafish that when imaged using confocal microscopy, would have a floor plate with some cells that couldn't produce SCOspondin but some that could. Then, I could look at the Reissner fiber and see what, if any, effects this would cause.

On a phenotypic level, where body axis curves are quantified, I observed 0% curly tail down fish at the 0 pg/nl concentration, which is expected given this condition is the negative control with no gene disruption. At 10 pg/nl, I observed a curly tail down phenotype rate of 0.89%. At 100 pg/nl, I observed a phenotype rate of 90.9%. At 500 pg/nl and 1000 pg/nl, the phenotype rates were both 100%. This indicates that the most critical window for inducing significant defects in body axis morphology is somewhere within the range 10-100 pg/nl, since these two concentrations demonstrated either largely curved (100pg/nl) or straight (10pg/nl)

body morphologies. Further tests by my postdoctoral mentor, Beth Bearce, revealed that at levels between 10-100 pg/nl where there was a bimodal distribution in body phenotype, all fish that were injected within this range demonstrated visible mosaicism at the tissue level in the medial floorplate. This suggests that a crispant strategy like ours which is injected at the 1-cell stage works quite quickly on early dividing tissues and affects the bulk of cells in the embryo when concentrations of guides are sufficiently high enough to work at all.

The 10 pg/nl and 100 pg/nl injections provided the most intriguing results with respect to Reissner fiber assembly. Even though these fish were either curvy or straight, they had visible mosaicism where Sspo-GFP fluorescence remained intact in small clusters (typically 1-5 cells) peppered along the central canal (figure 3, panels a-h). For example, panels a,c, and d show that despite several fluorescent floor plate cells expressing Sspo-GFP, there is no visible Reissner fiber, showing that expression from these cells was not sufficient to assemble a fiber. In contrast, panels b, e, f, g, and h show that despite visible disruption to portions of floor plate cells, a Reissner fiber was able to form albeit with compromised integrity compared to the Reissner fiber of the zebrafish injected with only crispant cocktail (0 pg/nl). It is also important to note that the presence of a Reissner fiber did not guarantee a straight body axis. For example, the central canal shown in panel f is taken from a bent fish despite having a Reissner fiber (notably it appears of compromised integrity).

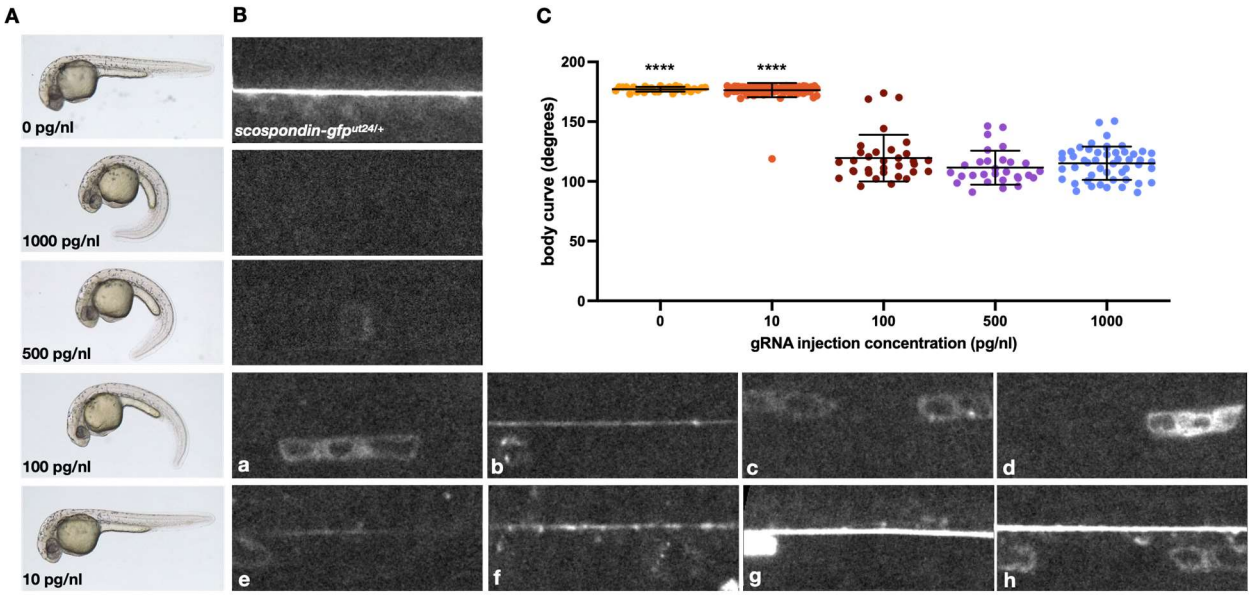

Figure 3: (A-C) Phenotypic, microscopic, and quantitative data from *scospondin-GFP*^{ut24} mosaic mutants.

A) Lateral views at 28hpf of each injection condition.

B) Confocal microscopy fluorescent images of the central canal of zebrafish within each injection condition. Note that for 0 pg/nl, 1000 pg/nl, and 500 pg/nl, there is only one panel showing that condition because results were redundant. However, due to unique results at the 100 pg/nl and 10 pg/nl condition, additional panels are shown and all are individually labeled (a-h) for reference in results.

C) Superplot body angle measurements for each injection condition. Individual dots represent the body angle of an individual embryo at 28hpf, and black bars represent the mean ± SD. **** indicates 0 pg/nl and 10 pg/nl were significantly different from 100 pg/nl, 500 pg/nl, and 1000 pg/nl conditions ($p<0.0001$). Conditions at 0 and 10 were not significantly different from each other. UI = uninjected.

Discussion

In these experiments, I first sought out to identify if F-spondin proteins are important to the zebrafish Reissner fiber and the body straightening process. Based on three rounds of injections into the AB (wild type) strain of zebrafish, there were no phenotypic differences

between zebrafish lacking F-spondin proteins and control zebrafish. Notably, the experiment did work because *sspo* crispants did have a statistically significant body angle defect, providing a positive control. This demonstrates that Spon1a and Spon1b do not appear to play a role in axial straightening because zebrafish lacking these proteins did not develop phenotypes.

In the *scospondin-GFP^{ut24}* zebrafish line, Spon1a and Spon1b mutations were also induced in order to visualize the integrity of the Reissner fiber in these crispants. Interestingly, there was more phenotypic variability when Spon1a and Spon1b mutations were induced in this line over AB zebrafish. The reason that more phenotypes were observed when mutations were induced in the *scospondin-GFP^{ut24}* line over the AB line is unclear. One potential explanation is that the GFP protein had an unintended interaction with SCOspondin in the Sspo-GFP line, which may slightly impact the integrity of the fiber such that the system is more predisposed to defects in this genetic background. Another explanation is that F-spondin proteins do play a role in axial straightening, but there is a compensatory mechanism that most zebrafish have to protect against a lack of these proteins. Perhaps the few zebrafish in this line that did have phenotypes lacked substantial compensation for stochastic reasons. However, given the strong effect observed in the AB line, overall, I conclude that Spon1a and Spon1b are not required for axial straightening or the integrity of the Reissner fiber despite being a component of the fiber. It is also true that I may not have sufficiently mutated Spon1a and Spon1b in my crispant experiments to induce a potential gross phenotype. As such, it will be important in the future to generate germline *spon1a* and *spon1b* single and double mutants to completely rule out a role for these genes in body axis formation.

To investigate the local dynamics of Reissner fiber assembly, I also generated mosaic mutants that lacked SCOspondin expression in some floor plate cells but not others. First, this

experiment showed that on phenotypic level, fish were mostly either straight or curly tail down with few exceptions. Very rarely did I observe intermediate axis curvature despite a range of mosaicism at the level of floor plate Sspo-GFP expression. Indeed, almost all of the fish at the lowest injection conditions of 10 pg/nl and 100 pg/nl had a central canal that was peppered with portions of floor plate cells that expressed Sspo-GFP and portions that didn't. In some cases, like in panel a or d of figure 3, the material produced by these functioning cells was not enough to form a Reissner fiber. Correspondingly, these fish failed axial straightening. This demonstrates that there is likely a threshold concentration of SCOspondin that is necessary to form a Reissner fiber, supporting my hypothesis that sufficient SCOspondin is needed at a local level to form a fiber. In contrast, panel g shows that despite only one floor plate cell that is expressing Sspo-GFP, there is a robust Reissner fiber. Further, panel e shows a dim Reissner fiber despite little floor plate fluorescence. These two examples show that the fiber can still form across regions of Sspo-negative floor plate cells, supporting the idea that motile cilia generated fluid flow may negate local disruptions to SCOspondin production. Therefore, Reissner fiber assembly seems to rely on two aspects, an overall threshold of concentration that if reached a fiber can form, and distributed assembly. Further, in some embryos, an intact fiber was not sufficient to induce body straightening (panel f), showing that the Reissner fiber may require a certain level of SCOspondin accumulation to induce appropriate downstream signaling. Therefore, sub-optimal fibers may form but cannot function to straighten the axis.

My results provide important insights into the dynamics of the Reissner fiber that can be used to generate further hypotheses and research questions. For example, now that we know a threshold concentration of SCOspondin is necessary to form a fiber, future research should quantify more exact threshold concentrations and how many floor plate cells are needed to form

a fiber. Combining such genetic work with structural approaches to understand how SCOspondin, and other components, link together to form the fiber will be important for a full understanding of fiber assembly.

Chapter II: Investigating Factors Downstream of the Reissner Fiber

Introduction

Urotensin-II Peptides

Throughout Chapter I, we learned that proper body development depends on motile cilia, CSF flow, and an intact Reissner fiber. However, this doesn't elucidate what comes downstream of these processes to promote axial straightening. Particularly, how interactions between the Reissner fiber and CSF-cNs promote axial straightening are not precisely understood. Urotensin-II neuropeptides (Urps) have recently emerged as potential candidates to act downstream in this model of axial straightening[4]. Zebrafish have two Urps, Urp1 and Urp2, which are 10-amino acid peptides secreted by CSF-cNs[18,19]. In humans, they have been linked to heart disease and mental illness[20,21]. In a cilia motility mutant, Urp expression is downregulated and injection of Urp1 was able to rescue the ventral curves in these mutants[22]. These experiments suggest that Urps act downstream of CSF flow signals generated by motile cilia.

It is not entirely clear what causes CSF-cNs to upregulate Urps. One idea is that the mechano-sensory connection between the Reissner fiber and CSF-cNs may trigger CSF-cNs to fire and upregulate Urps[11]. However, the leading model is that the Reissner fiber aids transport of epinephrine to CSF-cNs, causing these neurons to fire and upregulate Urps. Support for this comes from studies that show exogenous epinephrine can rescue ventral body curves in zebrafish lacking a Reissner fiber[23]. Upon secretion from CSF-cNs, Urps bind to their receptor Uts2r3 which is expressed in the dorsal muscle fibers[2]. Therefore, this signaling pathway may promote dorsal slow twitch muscle contractions to correct ventral body curves and promote the development of a straight body axis[4].

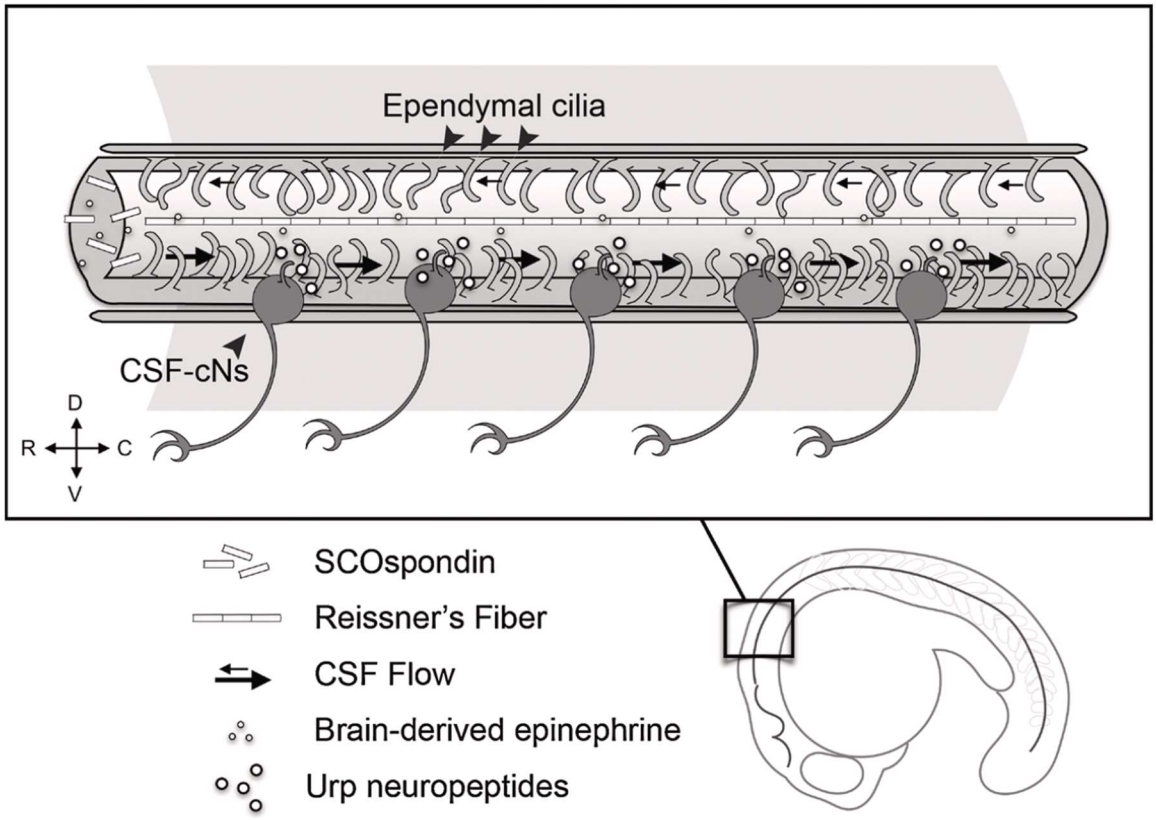

Figure 4: Schematic of the current model of axial straightening

Schematic of the current model of axial straightening. Motile cilia line the central canal of the spinal cord and generate CSF fluid flow. The fluid flow helps assemble to Reissner Fiber from SCOspondin, secreted by the sub commissural organ and floor plate cells. The Reissner Fiber assists transport of brain-derived epinephrine to signal to CSF-cNs. CSF-cNs then secrete the neuropeptides, Urps, which signal to dorsal muscle fibers through their receptor Uts2r3. Image source: Bearce, 2020[4].

My Work

Given that Urps have emerged as likely signaling proteins in axial straightening, my goal was to address how these peptides function in both early axial straightening and later growth phases to maintain a straight spine. To accomplish this, my lab generated several zebrafish mutant lines lacking Urp1, Urp2, and both Urp1 and Urp2, or the urotensin receptor (Uts2r3). A group of these mutants was followed at 1-2 days post fertilization (dpf) in order to track early body straightening while another group was followed through adolescent growth stages (5-17

dpf). A third group of mutants was followed into adulthood to track the maintenance of a straight spine. These mutants were allowed to develop into adulthood before performing micro-computed tomography to visualize the spine. Given that urotensin peptides appear to function downstream of motile cilia generated fluid flow, I hypothesized that these zebrafish mutants would not undergo normal axial straightening and show ventral body curves that would persist into later growth stages, similar to cilia motility mutants.

Methods

Zebrafish

Zebrafish embryos were attained from natural mating of the AB strain. Experiments were approved by the University of Oregon Institutional Animal Care and Use Committee and followed the guidelines of the International Association for Assessment and Accreditation of Laboratory Animal Care. The zebrafish lines generated to investigate the role of urotensin peptides were *urp1*$^{\Delta P}$, *urp2*$^{\Delta P}$, *urp1*$^{\Delta P}$*;urp2*$^{\Delta P}$, and *uts2r3*^{b1436} (ΔP refers to mutation to the peptide coding regions of these genes). The mutant lines *cfap298*^{tm304} (lacking a protein necessary for cilia motility) and *sspo*^{b1446} (lacking the protein SCOspondin) were also generated as positive controls. Crispants were also generated and compared to the mutant lines with germline mutations. The crispants are referred to as *urp1, urp2, urp1;urp2, cfap298,* and *sspo.*

gRNA Synthesis and CRISPR/Cas9 Mutagenesis

A look-up table provided the 4 gRNA oligos for *urp1*, *urp2*, *cfap298*, and *sspo* somatic mutagenesis[17].

urp1 oligo sequenc	5'/TAATACGACTCACTATAGGGAAAATAAATAACATGGTGTTTTAGAGCTAGAAATAGC/3';

es:	5’/TAATACGACTCACTATAGGTTCAGAAGCTGGTAGCAGGTTTTAGAGCTAGAAATAGC/3’; 5’/TAATACGACTCACTATAGGACACGGCTCTGCCACAACGTTTTAGAGCTAGAAATAGC/3’; 5’/TAATACGACTCACTATAGGAAAGTGAAGATCGCGGCCGTTTTAGAGCTAGAAATAGC/3’
urp2 oligo sequences:	5’/TAATACGACTCACTATAGGTCACCAGGTAGTGACGGAGTTTTAGAGCTAGAAATAGC/3’; 5’/TAATACGACTCACTATAGGTGGACACGAGGAGACCGAGTTTTAGAGCTAGAAATAGC/3’; 5’/TAATACGACTCACTATAGGGACATTTCCTGACGGAGAGTTTTAGAGCTAGAAATAGC/3’; 5’/TAATACGACTCACTATAGGTGACTGTCGCTTCAATCGGTTTTAGAGCTAGAAATAGC/3’
cfap298 oligo sequences:	5’/TAATACGACTCACTATAGGTTCTCTTCAACACTACGGGTTTTAGAGCTAGAAATAGC/3’; 5’/TAATACGACTCACTATAGGGCTCCACAATCTGATCATGTTTTAGAGCTAGAAATAGC/3’; 5’/TAATACGACTCACTATAGGGCTCCACAATCTGATCATGTTTTAGAGCTAGAAATAGC/3’; 5’/TAATACGACTCACTATAGGTCTCTGGCAGGTGCGCCCGTTTTAGAGCTAGAAATAGC/3’

Guide RNAs were generated for each target by first assembling oligos. First, equimolar concentrations of top oligos (10 µM each) were mixed. In a PCR strip, 1 µL of the diluted top oligos was mixed with 0.5 µL Phusion DNA polymerase, 25 µl 2x Phusion buffer +dNTPs, 22.5 µl nuclease-free water, and 1 µl of the bottom strand ultramer (10 µM). The oligo was then annealed and extended using a thermocycler with the following protocol: 98°C (2 min), 50°C (10 min), 72°C (10 min), 4°C (hold).

The assembled oligos were then purified using a Zymo Research DNA Clean & Concentrator-5 kit. After, the purified, assembled oligo was used for *in vitro* RNA synthesis using a NEB T7 High Yield kit. After four hours of incubation at 37°C, 1 µL of DNase was added and allowed to incubate for 15 minutes. The gRNA was purified using an RNA Clean & Concentrator Kit from Zymo Research. Individual aliquots of 3 µL each gRNA were stored at -80°C until use. For the use in mutagenesis, 1000 pg of gRNAs and1600 pg/nl Cas9 was injected into one-cell-stage embryos.

Quantifying Body Angles at early developmental timepoints

Using a Leica S9i stereomicroscope with an integrated 10-megapixel camera, lateral views of zebrafish larvae were taken at 28-30 hours post-fertilization (hpf). The body angles were determined utilizing ImageJ[24]. To follow adolescent growth stages, the same protocol was used but *urp1;urp2* mutants were imaged each day through 5-17 dpf.

X-ray microcomputed tomography

Using a vivaCT 80 (Scanco Medical), zebrafish were scanned at voxel resolutions of 18.5 µm (for 3 mpf and 12 mpf fish) or 10 µm (for 1 mpf fish)[25] and digital dissections of the spinal column were carried out using 3D Slicer and the Segmentation Editor. In the axial slice view, a threshold value of 3200 was applied to create a mask that outlined a 1 mm tube around the spine. This tube extended from the otic vesicles rostral to the first vertebrae to the split of the tail, with its center positioned at the narrowest 'hollow' within the lumen of the centra.

Quantification of lateral spine curvature

Image J was used to quantify the spinal curves of adult zebrafish. Cobb Angle measurements were taken by measuring the angle between the most displaced vertebral elements at the beginning and end of the curve according to established protocol[25].

Results

Urp1 and Urp2 are dispensable for embryonic axial straightening

To investigate the role of Urp1 and Urp2 in early axial straightening, we generated germline mutants lacking these peptides. We induced mutations through CRISPR/Cas9 mutagenesis to generate *urp1*$^{\Delta P}$ and *urp2*$^{\Delta P}$ mutant lines. Both of these lines displayed normal axial straightening (figure 5). We compared these germline mutants to the crispants *urp1* and *urp2* and showed that crispants phenocopied their germline counterpart (figure 5). The germline mutants *urp1*$^{\Delta P}$ and *urp2*$^{\Delta P}$ were compared to *cfap298*^{tm304} mutants that lack cilia motility in the central canal and *sspo*^{b1446} mutants that lack SCOspondin, the key component of the Reissner fiber. As expected *cfap298*^{tm304} *and sspo*^{b1446} mutants failed to undergo axial straightening and had the curly tail down phenotype (figure 5).

Given that Urp1 and Urp2 are structurally similar proteins, we also generated a double mutant line to investigate if these peptides act redundantly. If they do act redundantly in early axial straightening, then only by disrupting both proteins would we find a phenotype. However, we found that double mutants, deemed *urp1*$^{\Delta P}$*;urp2*$^{\Delta P}$*,* did not have a curly tail down phenotype and underwent proper axial straightening (figure 5). Additionally, we generated double mutants from adult female mutants; these mutants also exhibited normal axial straightening, showing that any potential maternally-derived *urp1* or *urp2* gene product does not function in axial

straightening. This demonstrated that Urp1 and Urp2 peptides are dispensable for axial straightening in early development.

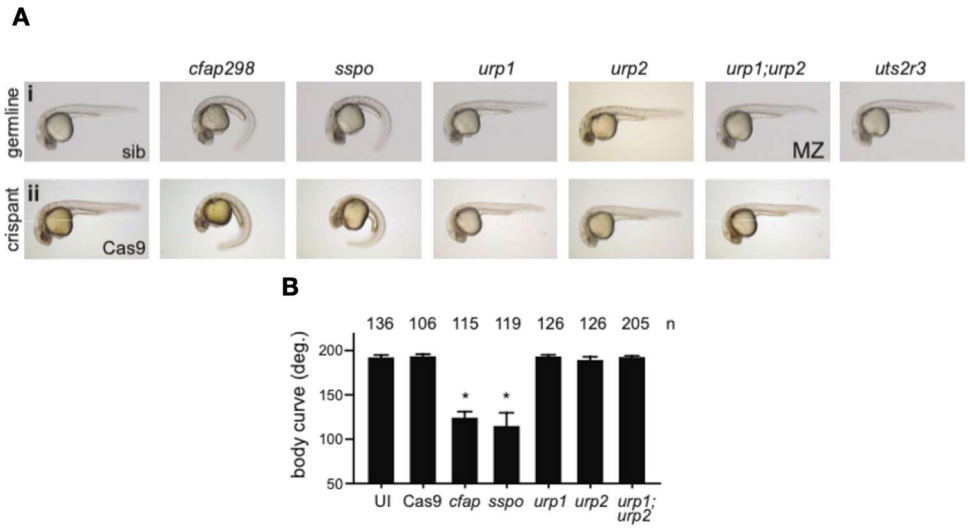

Figure 5: (A-B) Phenotypic and quantitative data from urotensin mutants compared to cilia motility mutants and Reissner fiber deficient mutants.

(A) Lateral views of germline mutants and crispants at 28-30 hfp compared to uninjected and Cas9-only injected controls. Mutants lacking Urps or the Urp receptor underwent axial straightening. Cilia motility (*cfap298*) or Reissner Fiber deficient mutants (*sspo*) failed axial straightening. (B) Body angles for crispants presented as mean ± standard deviation. UI = uninjected. *P<0.0001.

Urp1 and Urp2 are essential to maintain adult spine morphology

Although Urp1 and Urp2 are dispensable for axial straightening in embryonic zebrafish, we also investigated if these peptides are necessary for maintaining a straight spine throughout growth and aging. Therefore, we allowed mutant lines lacking one or both of these peptides to develop into adulthood and imaged them using X-ray microcomputed tomography. To quantify spinal curves, I used Cobb angle analysis which is a technique used in human scoliotic patients and measures deviations from straightness[25,26]. At 3 months post fertilization (mpf), *urp1*$^{\Delta P}$ mutants were normal, but *urp2*$^{\Delta P}$ mutants exhibited minor sagittal curves and kinked tails (figure

6). At 3 mpf, *urp1*$^{\Delta P}$*;urp2*$^{\Delta P}$ exhibited significant dorsal-ventral Cobb angles, particularly in the caudal region of the spine (figure 6 & 7). Therefore, Urp1 and Urp 2 function semi-redundantly in maintaining the adult spine because only by disrupting both proteins were severe curves observed. By comparing the *urp1*$^{\Delta P}$*;urp2*$^{\Delta P}$ double mutant to the *uts2r3*^{b1436} receptor mutant, we also found that the phenotypes were similar (figure 7), showing Urp1 and Urp2 likely signal through Uts2r3.

We also let another group of single *urp1*$^{\Delta P}$ and *urp2*$^{\Delta P}$ mutants age to 12 mpf to assess the role of these peptides in long term maintenance of spinal shape. In contrast to the absent or minor curves observed at 3 mpf, significant Cobb angles were observed in both of these mutants, but *urp2*$^{\Delta P}$ mutants had slightly more severe curves (figure 6). These mutants show the important role Urp1 and Urp2 play in maintaining correct spine shape throughout adulthood, with curves worsening over time.

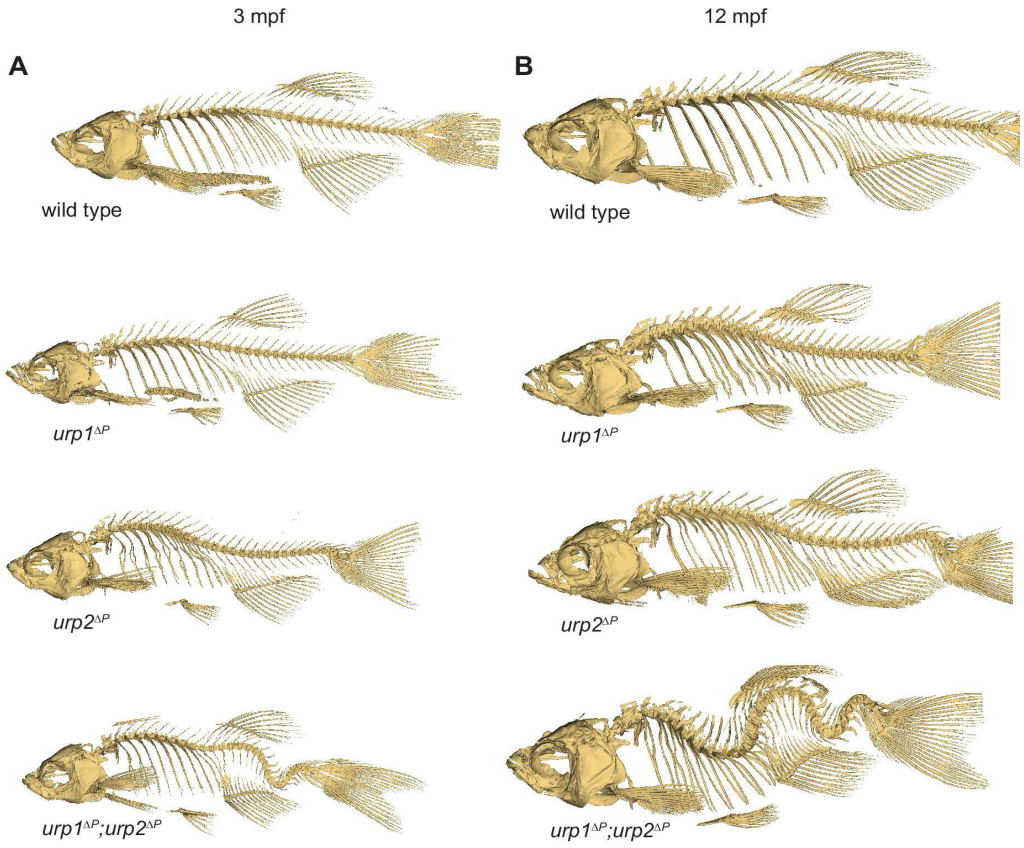

Figure 6: Spinal morphology of *urp1*$^{\Delta P}$ and *urp2*$^{\Delta P}$ single mutants *urp1*$^{\Delta P}$*;urp2*$^{\Delta P}$ double mutants at (A) 3 months post fertilization (mpf) and (B) 12 mpf

Urp1 and Urp2 play an important role in maintaining a straight spine through adulthood.

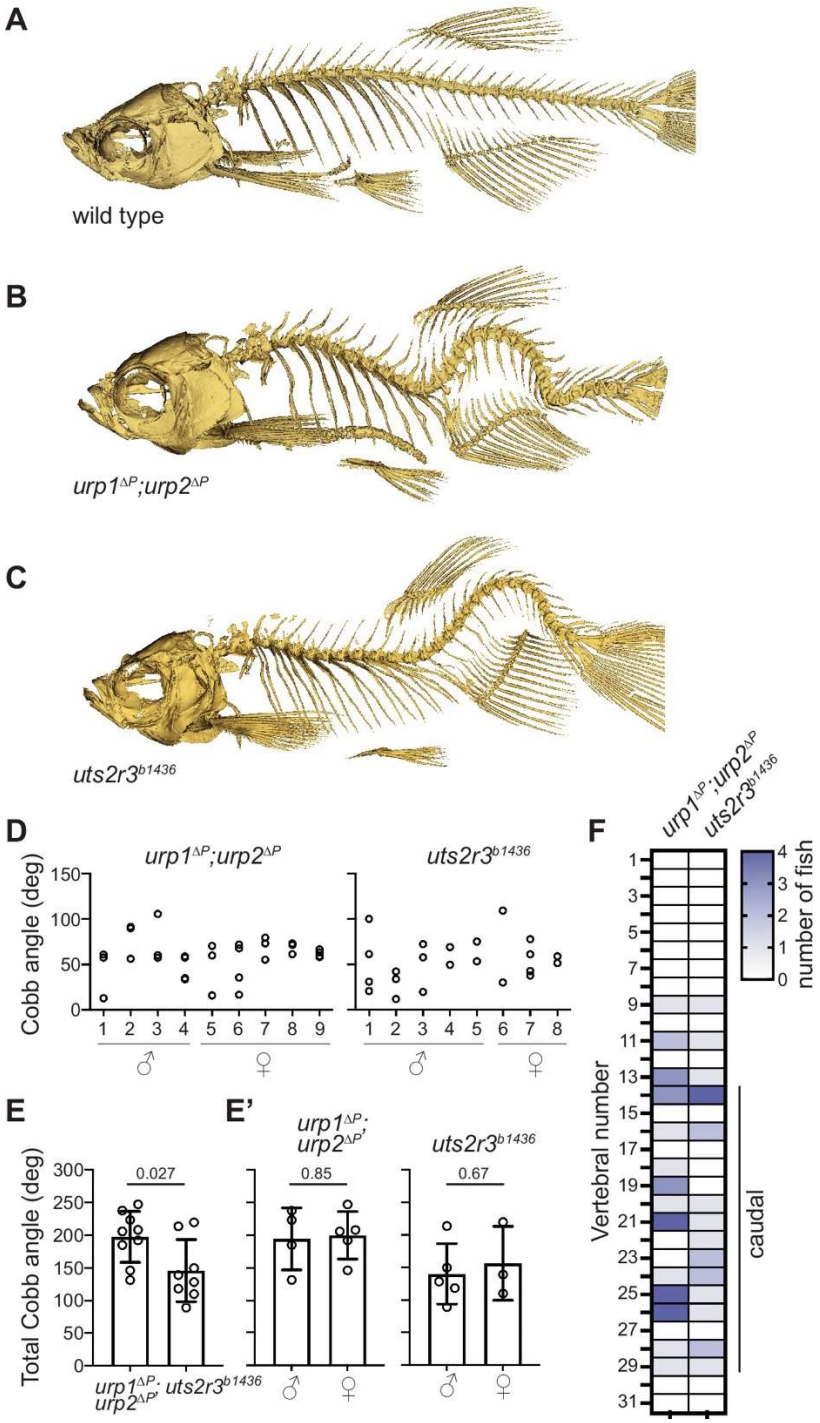

Figure 7: Phenotypic and quantitative data for urotensin deficient adult mutants

(A-C) show lateral views of adult wild type and mutants at 3mpf, showing the importance of Urp1 and Urp2 for proper spine morphology. (D) Individual Cobb angles plotted for each fish. (E-E') Total Cobb angles plotted as mean ± standard deviation. (F) Heat map of curve apex position, showing that most curves were located in the caudal region.

Spinal curves become apparent during adolescent growth phases

In the previous section, we found that adult zebrafish lacking urotensin peptides develop spinal curves that get progressively worse throughout adulthood. To determine when these curves started to develop, I performed a time course where I imaged *urp1*$^{\Delta P}$*;urp2*$^{\Delta P}$ double mutants as they developed. Curves first became apparent between 9-11 days which corresponds to adolescent growth phases in zebrafish (figure 8). At 13 days, all double mutants had noticeable curves, and these curves worsened till 17 dpf when the time course was ended (figure 8). These double mutants were also imaged through microcomputed topography at 3 mpf which showed that they did not have significant spinal defects like vertebral fusions. The lack of major vertebral defects shows that the spinal curves present in the double mutants were not due to congenital defects of vertebral patterning.

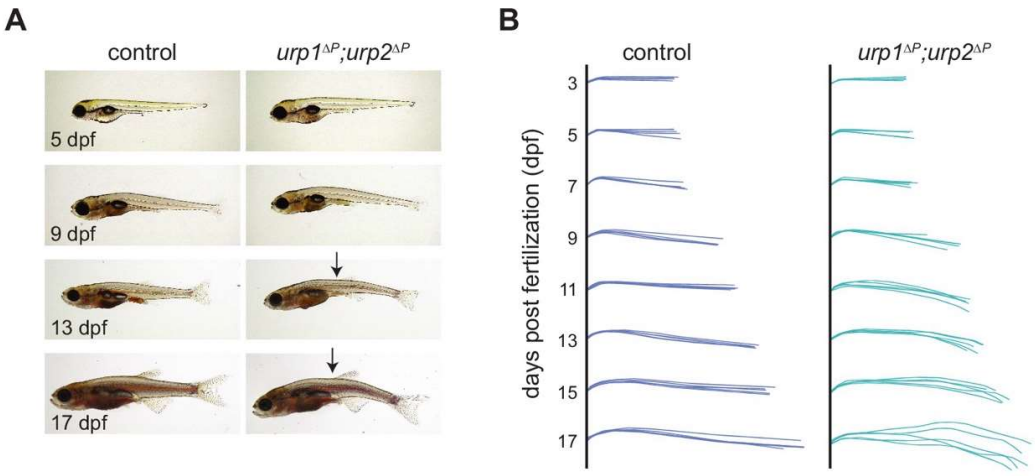

Figure 8: Phenotypic and curve-trace drawings for adolescent *urp1*$^{\Delta P}$*;urp2*$^{\Delta P}$ double mutants

(A) Lateral views of control and double mutants throughout adolescent growth phases. (B) Traces of body shape every two days through 3-17 dpf for both controls and double mutants. Curves become noticeable in every double mutant at 13 dpt.

Urotensin deficient mutants have distinct phenotypes compared to cilia mutants

Given that the current model of axial straightening in zebrafish is that urotensin peptides might function downstream of motile cilia generated flow and interactions between the Reissner fiber and CSF-cNs, we must compare the adult phenotype of *urp1*$^{\Delta P}$*;urp2*$^{\Delta P}$ double mutants to a cilia motility mutant (*cfap298*^{tm304}). If urotensin peptides are the factor driving body straightening downstream of motile cilia generated CSF flow, *urp1*$^{\Delta P}$*;urp2*$^{\Delta P}$ double mutants and *uts2r3*^{b1436} mutants should phenocopy *cfap298*^{tm304} mutants. To compare these phenotypes, we imaged adults at 3 mpf using microcomputed tomography and performed dorsal-ventral Cobb angle analysis. Cobb angle analysis showed that *cfap298*^{tm304} mutants had more severe curves (average Cobb angle: 260.4±32.7°) than *urp1*$^{\Delta P}$*;urp2*$^{\Delta P}$ mutants (197.5±38.9°) or *uts2r3*^{b1436} mutants (146.1±47.4°). Additionally, *cfap298*^{tm304} showed pre-caudal curves in addition to caudal curves and had significant lateral curvature of the spine (figure 9). In contrast, *uts2r3*^{b1436} mutants and *urp1*$^{\Delta P}$*;urp2*$^{\Delta P}$ mutants had planar dorsal-ventral curves (figure 9). Taken together, these results show a distinct phenotype between cilia motility mutants and urotensin deficient mutants, showing that downregulation of urotensin peptides is not sufficient to explain the spinal curves observed in *cfap298*^{tm304} mutants. Likely, additional factors function downstream of cilia-generated CSF flow.

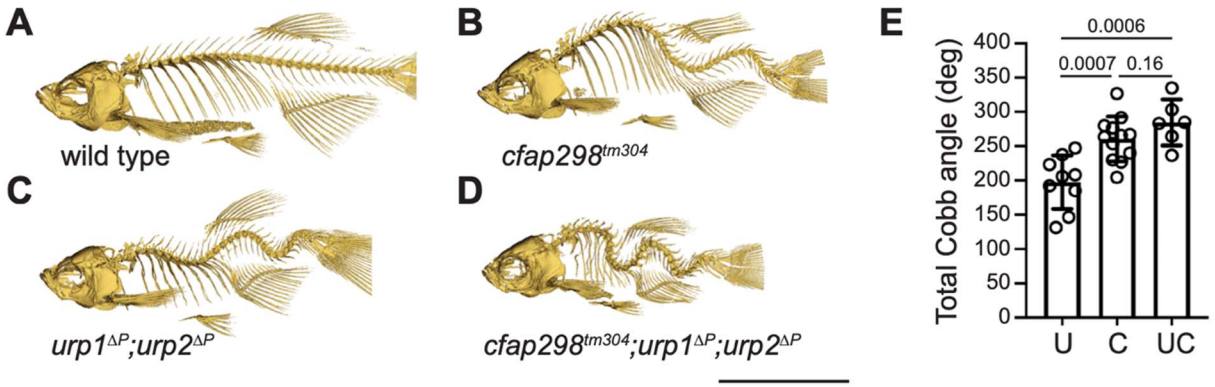

Figure 9: Phenotypic and quantitative data showing the distinct phenotypic in urotensin mutants

(A-D) Lateral views of (A) wild type, (B) *cfap298*^{tm304} mutants, (C) *urp1*$^{\Delta P}$*;urp2*$^{\Delta P}$ mutants, and (D) *cfap298*^{tm304}*;urp1*$^{\Delta P}$*;urp2*$^{\Delta P}$. (E) Total Cobb angles plotted as mean ± standard deviation. U = *urp1*$^{\Delta P}$*;urp2*$^{\Delta P}$ mutants, C = *cfap298*^{tm304} mutants, UC = *cfap298*^{tm304}*;urp1*$^{\Delta P}$*;urp2*$^{\Delta P}$.

To determine the genetic relationship between motile cilia and Urotensin peptides, we generated the triple mutant line *cfap298*^{tm304}*;urp1*$^{\Delta P}$*;urp2*$^{\Delta P}$. This mutant showed significant spinal curves similar to those in *cfap298*^{tm304} mutants (average total Cobb angle: 284.4±33.5°). These mutants, like cilia motility mutants, had dorsal-ventral and medio-lateral deviations in addition to pre-caudal curves (figure 9). Therefore, there may be multiple pathways driving spine morphology, one that relies on urotensin peptides and at least one more that doesn't.

Discussion

In Part II of this thesis, we set out to address the role of urotensin II peptides in early body development and also spinal shape maintenance throughout life. By generating mutant lines lacking Urp1 and Urp2, we showed that these peptides were dispensable for early axial straightening because these zebrafish underwent normal development, contradicting my earlier hypothesis. The dispensability of urotensin peptides is interesting because previous research showed that morpholino knockdown of Urp1/Urp2 resulted in the curly tail down phenotype[19]. Morpholino knockdown is where anti-sense oligonucleotides are injected into embryos to

transiently block gene expression by binding to RNA and inhibiting protein synthesis[27]. Therefore, the discrepancy between our mutants and morphants may be due to off-target effects of morpholino knock-down, but there are likely other factors that explain the discrepancy between mutants and morphants that need to be parsed out.

Despite urotensin deficient zebrafish undergoing normal early development, both single and double mutants started developing curves in adolescence. These curves got progressively worse throughout adulthood, demonstrating the role of urotensin peptides in maintaining spinal shape throughout life. However, these mutants were phenotypically distinct from cilia motility mutants. Cilia motility mutants have dorsal-ventral curves and medial-lateral spinal curves. However, urotensin deficient mutants only have dorsal-ventral curves, lacking the three-dimensional spinal curves that cilia motility mutants have. This discrepancy might provide evidence that there are separate systems mediating spinal shape. For example, Urp1 and Urp2 might mediate spinal shape in the ventral and dorsal directions while other factors may mediate spinal shape in the medial-lateral direction. Overall, the lack of a congruent phenotype between urotensin and motile cilia mutants shows that urotensin peptides are not the only downstream player in maintaining spinal shape. Therefore, there appears to be both urotensin dependent and urotensin independent factors controlling spinal shape. Future research should investigate what specifically controls spinal shape in the medial-lateral direction and other general factors besides urotensin peptides that mediate spine morphology.

Despite the preponderance of evidence demonstrating the role of urotensin peptides in spinal morphology in zebrafish, it will be important to discern how relevant these peptides are to human development and conditions like scoliosis. A recent genetic study comparing patients with adolescent idiopathic scoliosis and healthy subjects found that mutations to the human

urotensin receptor, UTS2R, were significantly associated with adolescent idiopathic scoliosis[28]. Another recent study provided direct insight into urotensin signaling in humans by dissecting muscle tissue from both the convex and concave sides of the spinal curvatures in human scoliotic patients[29]. There was significantly more expression of UTS2R on the convex side of the curve as compared to the muscle extracted from the concave side[29]. This finding provides further evidence that abnormal urotensin signaling may play a role in human scoliosis.

Overall, it is exciting that by gleaning information from zebrafish, we are able to understand more about human disease. In the future, more studies will need to investigate how urotensin peptides function in human spine morphology.

Bibliography

1. Boswell, C. W. & Ciruna, B. Understanding Idiopathic Scoliosis: A New Zebrafish School of Thought. Trends in Genetics vol. 33 183–196 Preprint at https://doi.org/10.1016/j.tig.2017.01.001 (2017).

2. Xie, H., Li, M., Kang, Y., Zhang, J. & Zhao, C. Zebrafish: an important model for understanding scoliosis. Cellular and Molecular Life Sciences 79, 506 (2022.

3. Kimmel, C. B., Ballard, W. W., Kimmel, S. R., Ullmann, B. & Schilling, T. F. Stages of embryonic development of the zebrafish. Developmental Dynamics 203, 253–310 (1995).

4. Bearce, E. A. & Grimes, D. T. On being the right shape: Roles for motile cilia and cerebrospinal fluid flow in body and spine morphology. Seminars in Cell and Developmental Biology vol. 110 104–112 Preprint at https://doi.org/10.1016/j.semcdb.2020.07.005 (2021).

5. King, S. M. Axonemal Dynein Arms. Cold Spring Harb Perspect Biol 8, a028100 (2016).

6. Mitchison, H. M. & Valente, E. M. Motile and non‐motile cilia in human pathology: from function to phenotypes. J Pathol 241, 294–309 (2017).

7. Zhao, C. & Malicki, J. Genetic defects of pronephric cilia in zebrafish. Mech Dev 124, 605–616 (2007).

8. Grimes, D. T. et al. Zebrafish models of idiopathic scoliosis link cerebrospinal fluid flow defects to spine curvature. Science (1979) 352, 1341–1344 (2016).

9. Driever, W. Developmental Biology: Reissner's Fiber and Straightening of the Body Axis. Current Biology vol. 28 R833–R835 Preprint at https://doi.org/10.1016/j.cub.2018.05.080 (2018).

10. Cantaut-Belarif, Y., Sternberg, J. R., Thouvenin, O., Wyart, C. & Bardet, P. L. The Reissner Fiber in the Cerebrospinal Fluid Controls Morphogenesis of the Body Axis. Current Biology 28, 2479-2486.e4 (2018).

11. Orts-Del'Immagine, A. et al. Sensory Neurons Contacting the Cerebrospinal Fluid Require the Reissner Fiber to Detect Spinal Curvature In Vivo. Current Biology 30, 827-839.e4 (2020).

12. Grimes, D. T. Making and breaking symmetry in development, growth and disease. Development 146, (2019).

13. Klar, A., Baldassare, M. & Jessell, T. M. F-spondin: A gene expressed at high levels in the floor plate encodes a secreted protein that promotes neural cell adhesion and neurite extension. Cell 69, 95–110 (1992).

14. Akle, V. et al. F-Spondin/spon1b Expression Patterns in Developing and Adult Zebrafish. PLoS One 7, e37593 (2012).

15. Higashijima, S., Nose, A., Eguchi, G., Hotta, Y. & Okamoto, H. Mindin/F-spondin Family: Novel ECM Proteins Expressed in the Zebrafish Embryonic Axis. Dev Biol 192, 211–227 (1997).

16. Troutwine, B. R. et al. The Reissner Fiber Is Highly Dynamic In Vivo and Controls Morphogenesis of the Spine. Current Biology 30, 2353-2362.e3 (2020).

17. Wu, R. S. et al. A Rapid Method for Directed Gene Knockout for Screening in G0 Zebrafish. Dev Cell 46, 112-125.e4 (2018).

18. Sugo, T. et al. Identification of urotensin II-related peptide as the urotensin II-immunoreactive molecule in the rat brain. Biochem Biophys Res Commun 310, 860–868 (2003).

19. Zhang, X. et al. Cilia-driven cerebrospinal fluid flow directs expression of urotensin neuropeptides to straighten the vertebrate body axis. Nat Genet 50, 1666–1673 (2018).

20. Russell, F. Urotensin II in cardiovascular regulation. Vasc Health Risk Manag Volume 4, 775–785 (2008).

21. Bulbul, F. et al. New molecule in the etiology of schizophrenia: Urotensin <scp>II</scp>. Psychiatry Clin Neurosci 68, 133–136 (2014).

22. Zhang, X. et al. Cilia-driven cerebrospinal fluid flow directs expression of urotensin neuropeptides to straighten the vertebrate body axis. Nat Genet 50, 1666–1673 (2018).

23. Lu, H., Shagirova, A., Goggi, J. L., Yeo, H. L. & Roy, S. Reissner fibre-induced urotensin signalling from cerebrospinal fluid-contacting neurons prevents scoliosis of the vertebrate spine. Biol Open 9, (2020).

24. Schindelin, J. et al. Fiji: an open-source platform for biological-image analysis. Nat Methods 9, 676–682 (2012).

25. Bearce, E. A., Ricamona, B. T. B., Fisher, K. H., O'Hara-Smith, J. R. & Grimes, D. T. Visualization and quantitation of spine deformity in zebrafish models of scoliosis by micro-computed tomography. STAR Protoc 4, 102739 (2023).

26. of Orthopaedic Surgeons., A. A. Outline for the study of scoliosis. Instr Course Lect 5, (1948).

27. Timme-Laragy, A. R., Karchner, S. I. & Hahn, M. E. Gene Knockdown by Morpholino-Modified Oligonucleotides in the Zebrafish (Danio rerio) Model: Applications for Developmental Toxicology. in 51–71 (2012). doi:10.1007/978-1-61779-867-2_5.

28. Dai, Z. et al. Novel Mutations in UTS2R are Associated with Adolescent Idiopathic Scoliosis in the Chinese Population. Spine (Phila Pa 1976) 46, E288–E293 (2021).

29. Xie, H. et al. Ependymal polarity defects coupled with disorganized ciliary beating drive abnormal cerebrospinal fluid flow and spine curvature in zebrafish. PLoS Biol 21, e3002008 (2023).